© 2017. Published by The Company of Biologists Ltd | Development (2017) 144, 1554-1565 doi:10.1242/dev.140038

RESEARCH ARTICLE

Distinct and redundant functions of Esama and VE-cadherin during vascular morphogenesis

Loïc Sauteur*, Markus Affolter‡ and Heinz-Georg Belting‡

ABSTRACT

The cardiovascular system forms during early embryogenesis and adapts to embryonic growth by sprouting angiogenesis and vascular remodeling. These processes require fine-tuning of cell-cell adhesion to maintain and re-establish endothelial contacts, while allowing cell motility. We have compared the contribution of two endothelial cell-specific adhesion proteins, VE-cadherin (VE-cad/Cdh5) and Esama (endothelial cell-selective adhesion molecule a), during angiogenic sprouting and blood vessel fusion (anastomosis) in the zebrafish embryo by genetic analyses. Different combinations of mutant alleles can be placed into a phenotypic series with increasing defects in filopodial contact formation. Contact formation in *esama* mutants appears similar to wild type, whereas *esama*$^{-/-}$; *ve-cad*$^{+/-}$ and *ve-cad* single mutants exhibit intermediate phenotypes. The lack of both proteins interrupts filopodial interaction completely. Furthermore, double mutants do not form a stable endothelial monolayer, and display intrajunctional gaps, dislocalization of Zo-1 and defects in apical-basal polarization. In summary, VE-cadherin and Esama have distinct and redundant functions during blood vessel morphogenesis, and both adhesion proteins are central to endothelial cell recognition during anastomosis.

KEY WORDS: Angiogenesis, Anastomosis, Cell contact formation, Morphogenesis, Cell adhesion, Esam, VE-cadherin, Cdh5, Endothelial cell, Zebrafish

INTRODUCTION

Establishment and expansion of vascular beds is essential for embryonic development and growth. Vascular networks are formed by the outgrowth of new blood vessels in a process called sprouting angiogenesis and their subsequent connection to another vessel or sprout by anastomosis. At the cellular level, sprouting angiogenesis and anastomosis are characterized by a series of dynamic behaviors, which are tightly coordinated (reviewed by Betz et al., 2016; Wacker and Gerhardt, 2011). In response to pro-angiogenic signals, endothelial cells (ECs) are activated. They remodel their actin cytoskeletons and downregulate their junctional adhesion molecules, thereby permitting cell motility, while maintaining cell contacts to each other and to the parental blood vessel. Thus, fine-tuning the cellular responses to angiogenic cues is essential to maintain vascular integrity and apical-basal cell polarization during angiogenic sprouting and anastomosis.

The cellular mechanisms that underlie blood vessel morphogenesis have been analyzed in detail by *in vivo* time-lapse microscopy in the zebrafish embryo (reviewed by Betz et al., 2016; Schuermann et al., 2014). During the formation of segmental arteries (SeAs), two or more cells emigrate from the dorsal aorta (DA) and form an angiogenic sprout. This sprout grows out to the dorsal side of the embryo (Blum et al., 2008; Siekmann and Lawson, 2007), where the tips of two adjacent sprouts interconnect and form the dorsal longitudinal anastomotic vessel (DLAV) (Blum et al., 2008; Herwig et al., 2011). Upon anastomosis, the ECs switch back to a more quiescent state (Leslie et al., 2007).

During sprouting and anastomosis, ECs show very diverse behaviors. Tip cells in the nascent sprout migrate extensively and form numerous filopodia, whereas the following stalk cells undergo extensive cell and junctional elongation (Gerhardt et al., 2003; Phng et al., 2013; Sauteur et al., 2014). This characteristic stalk cell behavior extends the sprouts in the dorsal direction and leads to the formation of a multicellular tube. At the tip of the sprout, filopodia of neighboring tip cells establish contact and initiate anastomosis. Anastomosis entails a number of dynamic behaviors that ensure proper apical-basal polarization, establishment of a continuous endothelium and formation of a patent tube (Herwig et al., 2011; Lenard et al., 2013).

Many of the mentioned cellular activities, such as formation of filopodia and changes in cell shape, require dynamic regulation of the actin cytoskeleton (Phng et al., 2013). These activities need to be coordinated by endothelial cell-cell interactions likely to be mediated by adhesion proteins. We have previously shown that the EC-specific adhesion protein VE-cadherin (VE-cad/Cdh5) is required for coordinated stalk cell elongation during extension of the SeA sprout and that this function requires the interaction of VE-cad with the cortical F-actin network (Phng et al., 2015; Sauteur et al., 2014). Furthermore, it was shown that VE-cad is also important for anastomosis by facilitating the formation of interfilopodial contacts at the onset of anastomosis (Lenard et al., 2013). However, the lack of VE-cad does not prevent EC interactions, suggesting that additional adhesion molecules cooperate with VE-cad during EC recognition and adhesion.

One of the adhesion proteins expressed in an EC-specific manner is Esam (endothelial cell-selective adhesion molecule), which belongs to the JAM (junction adhesion molecules) family (Hirata et al., 2001; Nasdala et al., 2002). Unlike its JAM homologs, Esam has been shown to exhibit considerable adhesion properties and to be sufficient to generate efficient cell contacts, when expressed in heterologous cell aggregation assays (Hirata et al., 2001; Nasdala et al., 2002). Although the mouse knockout of Esam does not cause vascular defects during embryonic development (Ishida et al., 2003), we considered Esam a good candidate as a cooperative partner of VE-cad for cell type-specific adhesion during angiogenic sprouting and anastomosis.

Biozentrum der Universität Basel, Klingelbergstrasse 70, Basel CH-4056, Switzerland.
*Present address: Department of Biomedicine, University Hospital Basel, Hebelstrasse 20, Basel CH-4031, Switzerland.

‡Authors for correspondence (markus.affolter@unibas.ch; heinz-georg.belting@unibas.ch)

H.-G.B., 0000-0002-1538-4364

Received 23 May 2016; Accepted 28 February 2017

Development (2017) 144, 1554-1565 doi:10.1242/dev.140038

We have generated a frame shift mutation in the zebrafish *esama* gene using transcription activator-like effector nuclease (TALEN) technology (Cermak et al., 2011). Zebrafish *esama* mutants are homozygous viable and do not exhibit overt defects during vascular development. By contrast, by combining of *ve-cad* and *esama* mutant alleles, we show that loss of Esama aggravates the *ve-cad* phenotype and that both proteins function in different aspects of blood vessel morphogenesis.

RESULTS

Single filopodial contacts are sufficient to initiate interendothelial contacts

To analyze the cell behaviors at the onset of anastomosis in detail, we performed live-imaging using transgenic reporters to visualize filamentous actin (F-actin, *fli:Galff*^{ubs3}; *UAS:EGFP-UCHD*^{ubs18}, Sauteur et al., 2014) and cell membranes (*kdrl:mCherry-CAAX*^{s916}, Hogan et al., 2009), thus allowing us to follow filopodial dynamics at high temporal and spatial resolution (Fig. 1A; Movie 1). DLAV formation is initiated at around 30 hours post-fertilization (hpf), when tip cells of SeAs send out filopodia in anterior and posterior directions and start to engage with each other. At the same time, the tip cells maintain motility and their cell bodies come into close proximity.

Our analysis showed that filopodia (visualized with mCherry-CAAX) of adjacent cells touched one to three times but did not stabilize the contact at the first encounter (n=14 movies; Fig. 1A-C; Movie 1). Eventually, a filopodial contact was maintained and cytoskeletal components (EGFP-UCHD) were quickly recruited, presumably stabilizing the contact (Fig. 1D,E). The cells subsequently expanded their contact area and formed junctions (Fig. 1F). On some occasions, tip cells formed contacts over two filopodial touching sites (data not shown), which were then fused to a single, continuous anastomotic contact.

VE-cad is required for efficient contact formation

The establishment of properly patterned vascular networks via sprouting angiogenesis and anastomosis requires cell type-specific recognition as well as adhesion. In principle, both tasks can be accomplished by cell type-specific adhesion molecules. ECs express a number of general and cell type-specific adhesion proteins. Among them, VE-cad has been shown to be the major component of endothelial adherens junctions (AJs) (reviewed by Dejana and Vestweber, 2013; Lagendijk and Hogan, 2015). We therefore decided to analyze the behavior of tip cell filopodia in the absence of VE-cad function.

In agreement with earlier studies (Lenard et al., 2013; Montero-Balaguer et al., 2009), tip cells lacking VE-cad still extended filopodia towards each other (Fig. 2A; Movie 2). However, we observed that filopodial contacts were more transient than in wild-type embryos and that VE-cad-deficient tip cells required more than ten filopodial interactions to establish firm contacts (n=8 movies; Fig. 2B,C), compared with wild-type siblings, which required one to three filopodial interactions (n=14 movies). We were able to observe two scenarios in *ve-cad* morphants. Although single filopodial contacts were not sufficient to produce definitive contacts, the tip cells continued their forward movements and established contacts via their cell bodies. Alternatively, in instances when two or more filopodial contacts occurred simultaneously, these contacts were maintained and ultimately led to anastomosis (Fig. 2D-F). These observations indicate that lack of VE-cad reduces filopodial adhesion, rendering single contacts ineffective. However, when the initial contact areas were enlarged, either by multiple filopodial contacts or by direct cell body contacts, anastomosis eventually occurred, suggesting that the available adhesion proteins were sufficient to trigger the process.

Esama is expressed in the endothelium and sprouting SeAs

Given that in the absence of VE-cad, ECs are still able to form new cell-cell contacts during anastomosis in a cell type-specific manner, we reasoned that other adhesive components must contribute to this process. Furthermore, these proteins should be restricted to the endothelium, in order to be able to confer cell type specificity. Among the reported endothelial adhesion proteins, Esam is expressed mostly in the endothelium but is also found in platelets and megakaryocytes (Hirata et al., 2001; Nasdala et al., 2002). The zebrafish genome encodes two paralogs of Esam, *esama* and *esamb*. In zebrafish, *esama* expression has been reported in ECs, the endocardium and also in a subset of neurons in the brain, including the epiphysis/pineal gland (Wong et al., 2009). We confirmed the endothelium-specific expression of *esama*, whereas we observed only weak expression of *esamb* in the vasculature (Fig. S1A,B).

Although no obvious vascular defects have been reported for murine Esam mutants (Ishida et al., 2003), we reasoned that Esam might cooperate with VE-cad during cell type-specific recognition, even if VE-cad might be sufficient for endothelium-specific adhesion in the absence of Esam. To assess the individual and combined contribution of both proteins to endothelial contact formation, we generated targeted mutations in the zebrafish *esama* gene using TALEN technology (Cermak et al., 2011). The isolated *esama*^{ubs19} allele harbors a 10 bp deletion in exon 2, which leads to a premature stop codon, leaving only the first 37 amino acids intact (see Fig. S2A,B). We confirmed the absence of the protein by immunohistochemistry in homozygous *esama* mutant embryos, using an Esama-specific antibody (Sauteur et al., 2014), which targets the intracellular domain of the protein (compare Fig. S2D and E).

esama/*ve-cad* double mutants exhibit aggravated anastomosis defects

Heterozygous *esama*^{ubs19} carriers were crossed to obtain homozygous mutants for phenotypic analysis. Initial analyses of *esama* mutants did not reveal any obvious defects (compare Fig. 3A,B), and anastomosis occurs in a comparable manner to wild-type conditions, with two to five transient filopodial contacts before contact stabilization (n=26 movies; Fig. S3; Movie 3). Furthermore, homozygotes developed to fertile adults.

To elucidate a potential synergism of VE-cad and Esama in endothelial contact formation, we generated *esama/ve-cad* double mutant (dKO) embryos and examined the developing vasculature during angiogenic sprouting and anastomosis by time-lapse imaging. Although the DA did not display any obvious additional defects compared with *ve-cad* single mutants, we found that the defects in angiogenesis and anastomosis were strongly aggravated in the dKO (Fig. 3; Movies 4-7).

The most obvious defects we observed concerned angiogenic cell behavior, cell adhesion and the establishment of a continuous endothelium during DLAV formation. First, dKO ECs showed enhanced hyper-protrusive activity, with an increase of filopodia on tip and also on stalk cells (Fig. 3E,F). Second, we also found that interendothelial adhesion was further decreased in dKO when compared with *ve-cad* single mutants. This adhesion defect was reflected by a high incidence of tip cell detachments during SeA sprouting (43% of 190 SeAs in 38 movies of dKO embryos compared with 34% of 65 SeAs in 13 movies of *ve-cad* mutant

Development (2017) 144, 1554-1565 doi:10.1242/dev.140038

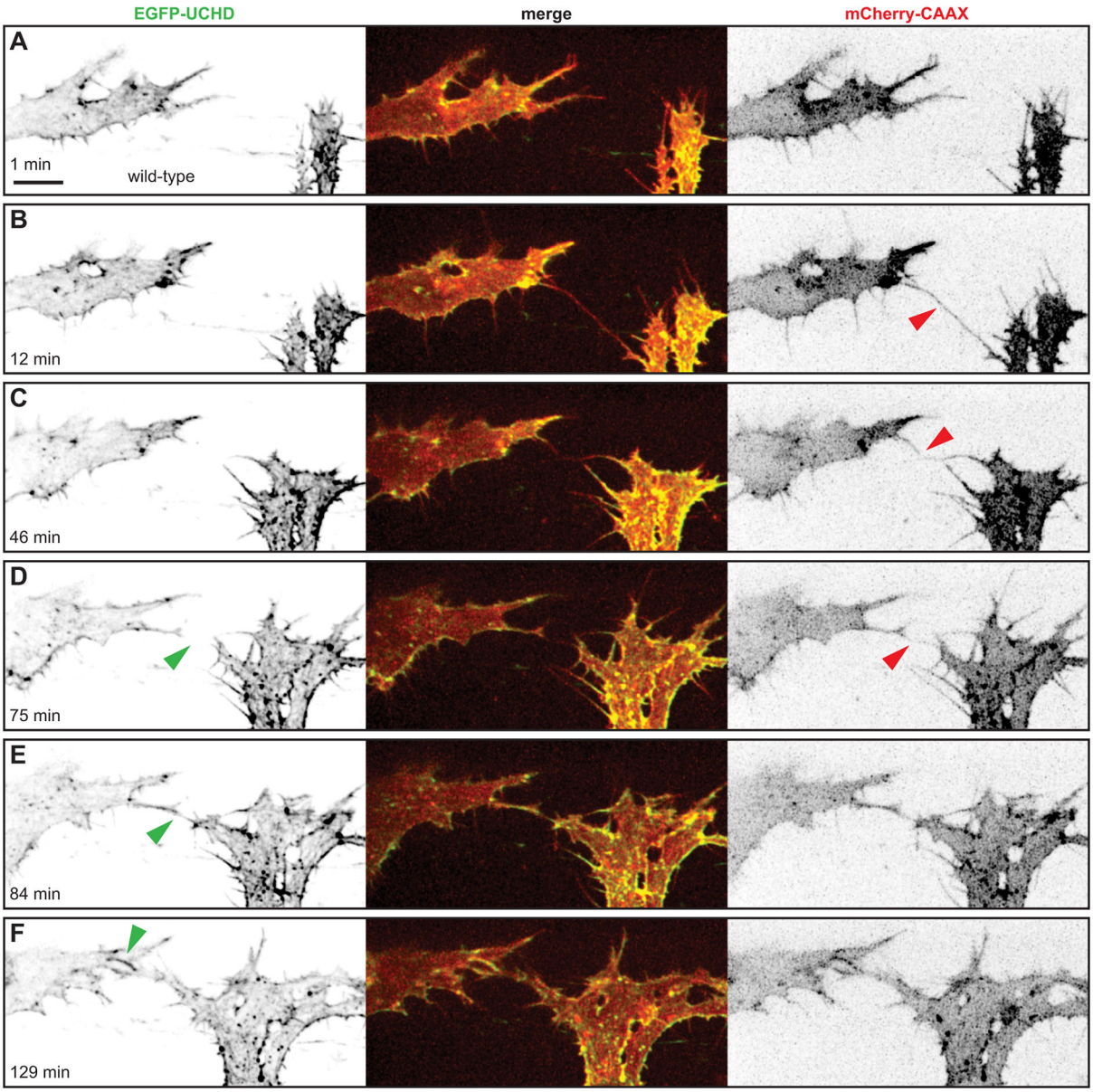

Fig. 1. Anastomosis occurs over a single filopodial contact. (A-F) Still images from Movie 1 of a Tg(*fli1ep:gal4ff*)^{ubs3}, Tg(*UAS:EGFP-UCHD*)^{ubs18}, Tg(*kdrl:mCherry-CAAX*)^{s916} embryo at around 32 hpf, with anterior to the left. Single channels are shown in inversed contrast (green is EGFP-UCHD and red is mCherry-CAAX on left and right, respectively) and the merge is shown in the middle. Red arrowheads point to filopodial interactions; green arrowheads point to cell-cell bridges or a junctional ring in (F). Scale bar: 10 µm.

embryos; Fig. 3C,D; Sauteur et al., 2014). Remarkably, *ve-cad* mutant stalk cells, which had detached from their leading tip cells, were generally able to reattach to the DLAV within 8 h after detachment. By contrast, only 37% of detached stalk cells of dKO embryos reattached to the DLAV (38 stalk cell detachments in 19 movies). Moreover, the tip cells normally making up the DLAV instead formed loose aggregates in dKO embryos (Fig. 3D″).

The last defect suggests that *esama/ve-cad* dKO ECs are incapable of generating stable interendothelial contacts and of forming an organized endothelium. To address this possibility, we crossed the *ve-cad* and *esama* mutant alleles into a transgenic reporter line, which simultaneously labels the cell membrane and F-actin in ECs. This allowed us to perform high-resolution time-lapse analyses of filopodial dynamics and EC interactions during anastomosis in dKO embryos (Fig. 4; Movie 8). Sprouting tip cells showed normal protrusive filopodial activity. However, and by contrast with wild-type embryos, the interactions between filopodia of neighboring tip cells did not lead to the formation of stable contacts. Instead, filopodia showed repetitive cycles of contact and retraction (n=20 movies). During transient filopodial contacts, we usually did not observe an accumulation of F-actin at these sites. Occasionally, when F-actin did accumulate, the tip cells were still not able to maintain these connections (Fig. 4B,C). Moreover, even when the two tip cell bodies came into direct contact, the connections were again only transient, and the tip cells later dissociated from each other (Fig. 4D,E). This behavior could occur several times between the same tip cells. Even when the tip cell eventually did overlap extensively and apparently joined more stably, the actin cytoskeleton did not form junctional ring structures, and consequently, the cytoskeleton appeared disorganized

Development (2017) 144, 1554-1565 doi:10.1242/dev.140038

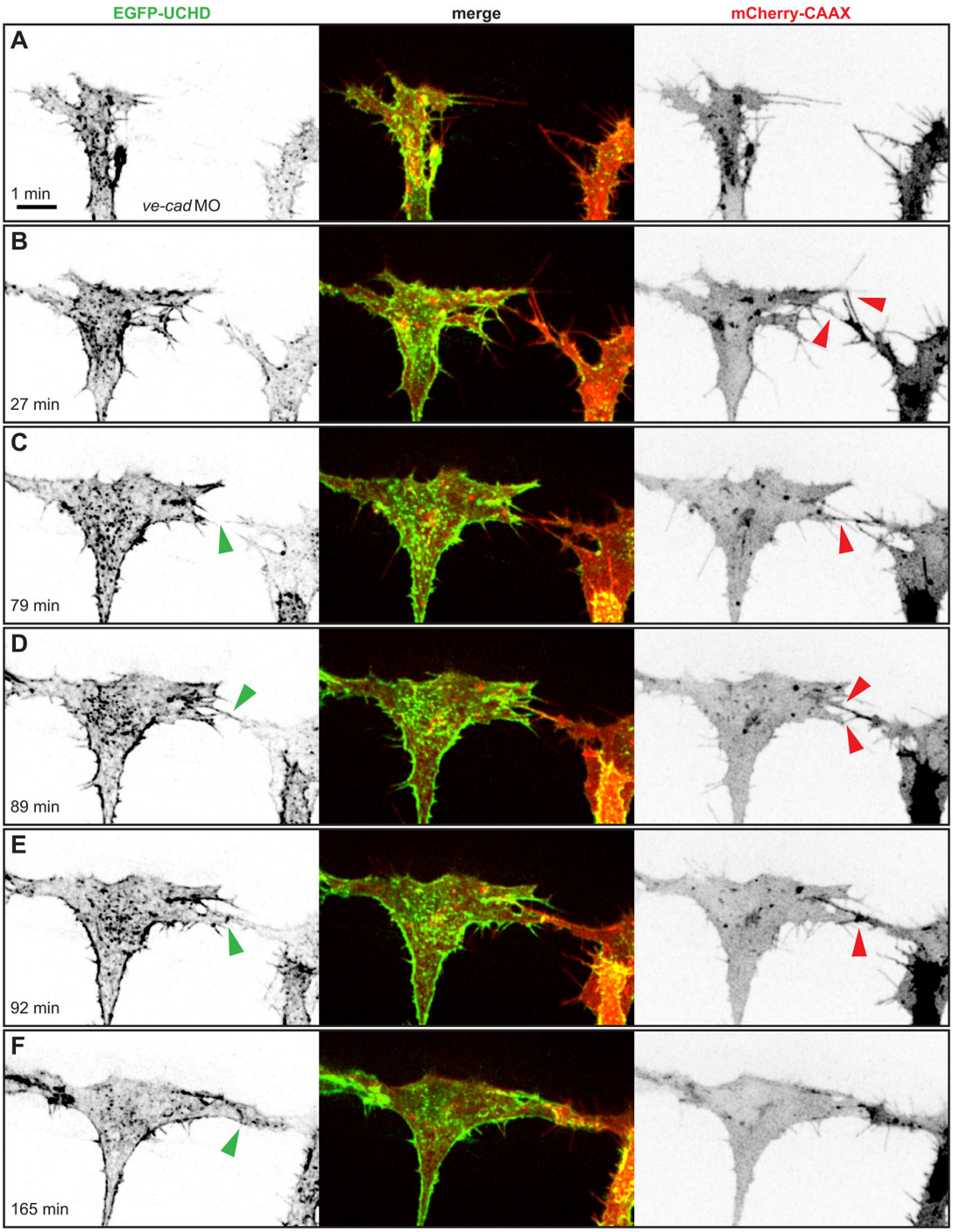

Fig. 2. In the absence of VE-cad, several filopodial contacts are required to initiate cell-cell contact formation. (A-F) Still images from Movie 2 of a VE-cad morphant Tg(*fli1ep:gal4ff*)^{ubs3}, Tg(*UAS:EGFP-UCHD*)^{ubs18}, Tg(*kdrl:mCherry-CAAX*)^{s916} embryo at around 32 hpf, with anterior to the left. Single channels are shown in inversed contrast (green is EGFP-UCHD and red is mCherry-CAAX on left and right, respectively) and the merge is shown in the middle. Red arrowheads point to filopodial interactions or cell bodies touching in (E); green arrowheads point to cell-cell bridges and forming junctions in (E) and (F). Scale bar: 10 µm.

compared with wild type (compare green arrowheads in Fig. 4F with Fig. 1F).

Taken together, these observations show that VE-cad and Esama are required to generate and maintain filopodial contacts, as well as general endothelial cell contacts during sprouting and, in particular, during anastomosis. Furthermore, our observation that remodeling of the F-actin network is disturbed in the dKO suggests that Esama/VE-cad-mediated adhesion is essential for the assembly of ECs into an organized endothelium.

Our results show that even though the loss of Esama alone has no effect on the ability of tip cell anastomosis, it drastically affects tip cell behavior in the absence of VE-cad. This phenotypic discrepancy between *esama*, *ve-cad* and dKO suggests a partly redundant role of both proteins during angiogenesis. Alternatively,

Development (2017) 144, 1554-1565 doi:10.1242/dev.140038

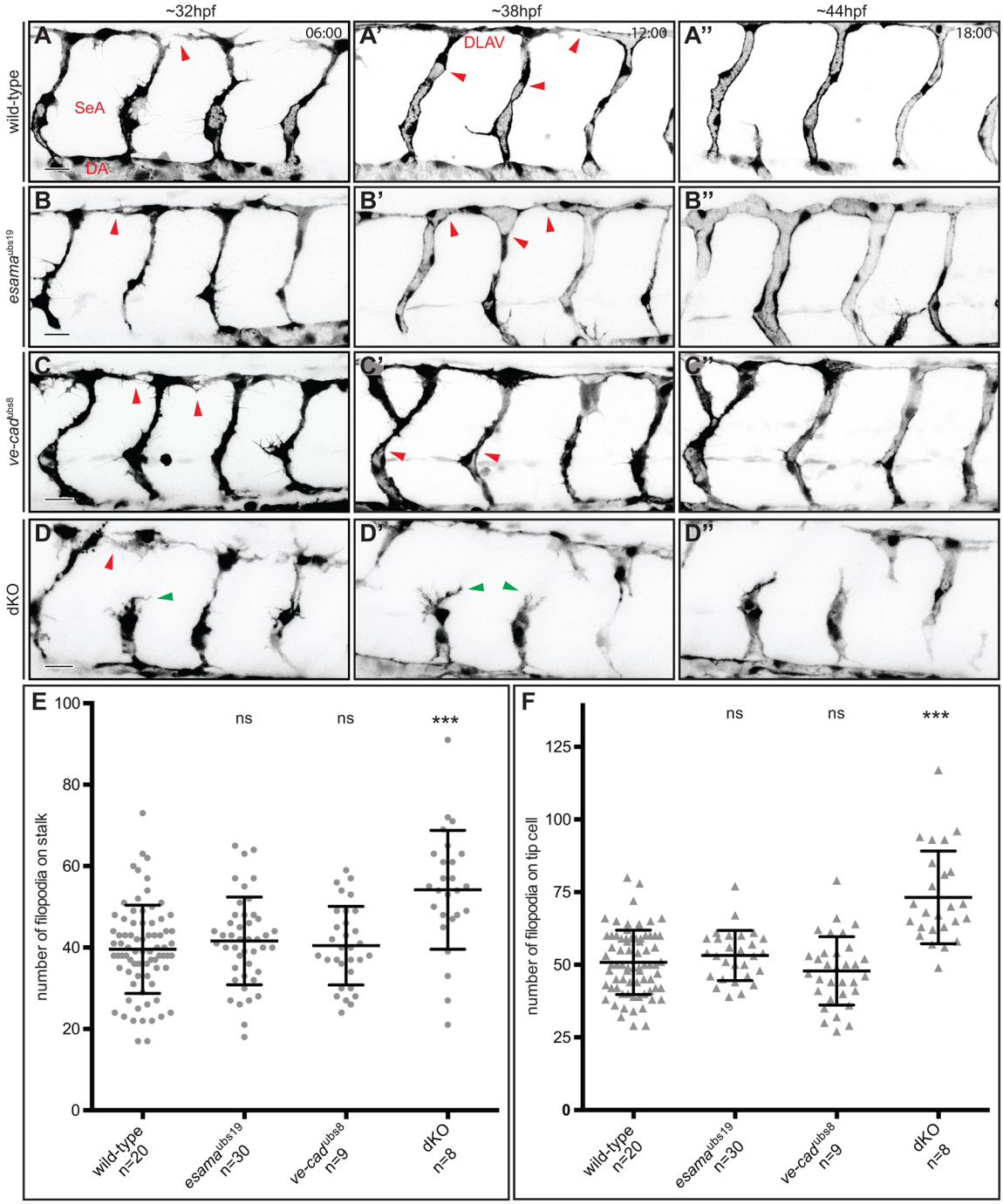

Fig. 3. Loss of both VE-cad and Esama enhances the defects observed in *ve-cad*^{ubs8} mutants. (A-D) Still images from Movie 4 (A), Movie 5 (B), Movie 6 (C) and Movie 7 (D) of Tg(*fli1a:EGFP*)^{y1} wild-type, *esama*^{ubs19}, *ve-cad*^{ubs8} and *esama*^{ubs19}; *ve-cad*^{ubs8} double mutant (dKO) embryos, respectively. Images are shown in inversed contrast at three different stages of angiogenesis: ~32, ~38 and ~44 hpf. Red arrowheads at 32 hpf point to anastomotic contacts; red arrowheads at 38 hpf point to forming lumen; green arrowheads point to stalk cells that detached from the tip cell. Scale bars: 20 µm. (E and F) Quantification of filopodial protrusions on SeA stalks (E) and tip cells (F). (E) The number of filopodia on angiogenic stalks (composed of one to three ECs) is comparable between wild-type (77 SeAs in *n*=20 embryos), *esama*^{ubs19} (114 SeAs in *n*=30 embryos) and *ve-cad*^{ubs8} (31 SeAs in *n*=9 embryos) genotypes. Significantly more filopodia were counted on dKO stalks (31 SeAs in *n*=8 embryos). (F) Tip cells generally generate more filopodial protrusions (average of 50 filopodia per tip cell) than stalk cells. Significantly more filopodia were counted on tip cells of dKO compared with wild type. Bars in the plots represent mean±s.d. DA, dorsal aorta; dKO, double mutant; DLAV, dorsal longitudinal anastomotic vessel; n, number of analyzed embryos; ns, not significant; SA, segmental artery. ***P<0.0001, with one-way analysis of variance (ANOVA).

the loss of *esama* function might be compensated by upregulation of *ve-cad* or *esamb*. We therefore compared the expression levels of *esama*, *esamb* and *ve-cad* in wild-type, *esama* and *ve-cad* mutant embryos (Fig. S1C). RT-qPCR analysis of 32 hpf embryos revealed that *esamb* mRNA levels were unchanged in *esama*, *ve-cad* and dKO mutants. For *ve-cad* mRNA, we observed a twofold increase in *esama* mutants, and likewise, in *ve-cad* mutants the levels of *esama* mRNA were increased twofold. Thus,

Development (2017) 144, 1554-1565 doi:10.1242/dev.140038

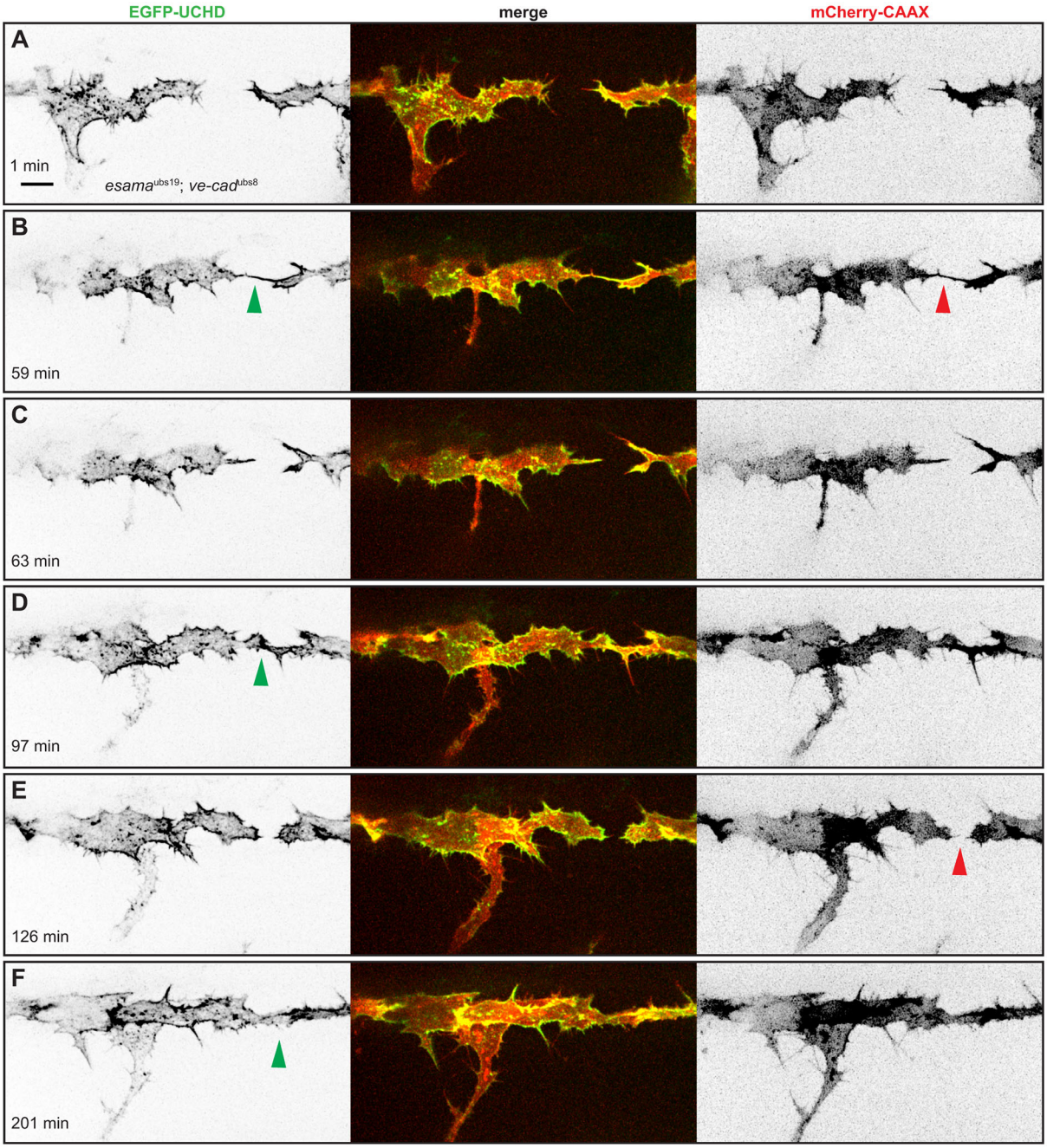

Fig. 4. *esama*^{ubs19}; *ve-cad*^{ubs8} double mutant tip cells cannot maintain cell-cell contacts. (A-F) Still images from Movie 8 of an *esama*^{ubs19}; *ve-cad*^{ubs8} double mutant Tg(*fli1ep:gal4ff*)^{ubs3}, Tg(*UAS:EGFP-UCHD*)^{ubs18}, Tg(*kdrl:mCherry-CAAX*)^{s916} embryo at around 32 hpf, anterior to the left. Single channels are shown in inversed contrast (green is EGFP-UCHD and red is mCherry-CAAX on left and right, respectively) and the merge is shown in the middle. Red arrowheads point to filopodial interactions (B) or resolved contacts (E); green arrowheads point to cell-cell bridges or forming junctions in (F). Scale bar: 10 µm.

elevated *ve-cad* mRNA levels might compensate for loss of Esama function in *esama* mutants.

To test further whether the *ve-cad* gene dose might modify the anastomosis process in the context of loss of Esama function, we performed time-lapse imaging on *ve-cad*$^{+/-}$; *esama*$^{-/-}$ mutants. Although these embryos are viable and fertile, they do show mild defects in cell-cell contact formation (Fig. S4; Movie 9). On average, these tip cells require seven filopodial contacts before achieving stable contacts (n=9 movies) compared with two to five in *esama* mutants and more than ten in *ve-cad* mutants, as shown above. These observations support our notion that VE-cad and Esama act redundantly during filopodial contact formation and that different levels of VE-cad influence the efficacy of filopodia to establish stable interendothelial contacts.

The role of Esama and VE-cad in DA formation and angiogenic sprouting

Given that we observed decreased cell-cell adhesion between stalk and tip cells as well as defects during cell-cell contact formation in dKO embryos, we addressed the junctional morphology in these embryos by examining the distribution of the scaffold protein Zo-1 (Tjp1a/b in zebrafish) during SeA sprouting. Furthermore, we

Development (2017) 144, 1554-1565 doi:10.1242/dev.140038

examined apical-basal polarization at EC contacts based on the localization of the apical protein Podocalyxin (Pdxl). Wild-type ECs in the DA showed a regular junctional pattern (Fig. S5A), and cross-sections through the DA showed a clear apical localization of Pdxl (Fig. S5A′). Furthermore, we observed the highest concentration of apical Pdxl in close proximity to cell junctions (red arrowheads in Fig. S5A). The junctional pattern of the DA in *esama* mutant embryos was indistinguishable from that in wild-type embryos (Fig. S5B), whereas the DA of *ve-cad* mutant embryos showed discontinuous lumens. The cell junctions of the DA in *ve-cad* mutants appeared irregular, indicating that the cellular organization of the tube was disturbed (red arrowheads in Fig. S5C). However, even in non-inflated regions, intercellular junctions were formed, and Pdxl localized apically between endothelial junctions (Fig. S5C′). Additional loss of Esama did not lead to an obvious additional morphological defect of the DA when compared with *ve-cad* single mutants (Fig. S5D,D′).

In striking contrast to the DA, the cellular architecture of SeA sprouts was much more strongly affected in dKO embryos. It is generally acknowledged that the activation of ECs by angiogenic stimuli leads to a decrease in endothelial cell adhesion and an increase in cell motility (Chaki et al., 2015; Dejana, 2004). Nevertheless, junctional localization of VE-cad, Esama and Zo-1 is maintained during SeA sprouting (Blum et al., 2008; Sauteur et al., 2014). When we examined Zo-1 distribution in sprouting SeAs in the absence of VE-cad and Esama, we found that Zo-1 was often lacking at cell borders, even between two obviously connected ECs (Fig. 5D). Moreover, the junctions that did form were often discontinuous and exhibited large intrajunctional gaps (red arrowheads in Fig. 5D″). Frequently, Zo-1 appeared delocalized in these cells and accumulated in the cytoplasm, suggesting a lack of available binding partners for Zo-1 at EC junctions (compare Fig. 5A″,D″, green arrowheads).

We have previously shown that the dorsal extension of SeAs is to a large extent accomplished by stalk cell elongation and that this processes requires VE-cad (Sauteur et al., 2014). Examination of junctional patterns revealed that this process was not affected in *esama* mutants (compare Fig. 5B and C). Despite this, *esama* single mutants showed small intrajunctional gaps, albeit much smaller than those we observed in dKO (red arrowheads in Fig. 5B″). These gaps were seen mostly in early steps of sprout extension, whereas they were absent in sprouts that had undergone lumen formation (see also Fig. 6B). When we compared the occurrence and extent of intrajunctional gaps in wild-type, *esama* and *ve-cad* mutants (Fig. 5E), we found that they were more frequent in *esama* than in *ve-cad* mutant embryos. In the absence of VE-cad, we counted approximately one intrajunctional gap per SeA, whereas they were almost twice as abundant in *esama* mutants. These differences point to non-redundant roles of Esama and VE-cad in sprouting SeAs. Esama is required during earlier steps of junction formation and maturation, whereas it is expendable at later stages of blood vessel formation. By contrast, VE-cad appears to be required primarily for dynamic junctional rearrangements.

Intrajunctional gaps are associated with defects in apical polarization

As cell junctions are thought to be essential for the separation of apical and basal membrane compartments of ECs (Lampugnani et al., 2010; Strilić et al., 2009, 2010), we wondered whether the appearance of intrajunctional gaps in *esama* and *ve-cad* mutants impacts apical-basal polarization. When we stained wild-type embryos for Zo-1 and the apical membrane marker Pdxl, we observed Pdxl to be contained within junctional rings (Fig. 6A). Likewise, in single mutants, Pdxl was confined to those membrane compartments that were enclosed by intact (i.e. not-interrupted) junctional rings (see base of sprouts in Fig. 6B,C). By contrast, in the context of intrajunctional gaps, Pdxl became delocalized and was also found in basal membrane compartments. Furthermore, the size of the junctional gaps was correlated with the degree of basal Pdxl localization (Fig. 6B″,C″) and became most obvious in dKO embryos (Fig. 6D). In dKO embryos, these junctional gaps were maintained during the entire process of SeA formation and were associated with defects in apical-basal polarization. By contrast, in *ve-cad* and *esama* single mutants, these gaps appeared only transiently and were not observed in later stage SeAs; in these vessels, Pdxl was restricted within the junctional rings.

DISCUSSION

Angiogenesis requires the tight regulation and coordination of interendothelial cell adhesion and motility. In this study, we have analyzed the individual and combined requirements of VE-cad and Esama during angiogenic sprouting and anastomosis. Although the importance of VE-cad for embryonic blood vessel formation is well documented (Carmeliet et al., 1999; Gory-Fauré et al., 1999; Montero-Balaguer et al., 2009; Sauteur et al., 2014; and reviewed by Lagendijk and Hogan, 2015), the role of Esam in this process is not clear. Previously, Esam has been implicated in neutrophil diapedesis and the etiology of several human diseases (Khandoga et al., 2009; Wegmann et al., 2006; and reviewed by Luissint et al., 2014). However, murine Esam null mutants are homozygous viable, and no vascular defects have been described (Ishida et al., 2003). This is in contrast to *in vitro* studies, which show that Esam has strong adhesive properties and suggest an important role in EC junction formation and maturation (Kimura et al., 2010; Nasdala et al., 2002). We therefore reasoned that the role of Esam *in vivo* might be obscured by the presence of other adhesion molecules with function at least partly redundant with Esam during embryonic angiogenesis. To explore this possibility, we generated a putative null allele of *esama* in zebrafish. In agreement with data from mouse mutants, homozygous *esama* mutants do not display overt vascular defects and are viable and fertile. Here we show, however, that when bred into the *ve-cad* mutant background, the additional loss of *esama* strongly aggravates the *ve-cad* single mutant phenotype, suggesting that Esama and VE-cad are at least partly redundant during blood vessel morphogenesis (see also Fig. S6).

Synergistic functions of Esama and VE-cad during blood vessel anastomosis

Cell type-specific recognition and adhesion between ECs are prerequisites for efficient blood vessel anastomosis. Both processes are mediated by the intercellular engagement of tip cell filopodia. However, recent *in vivo* studies have shown that lack of filopodia does not prevent sprout outgrowth and anastomosis and that tip cells can generate contacts between their cell bodies in the absence of filopodia (Phng et al., 2013). These findings are in agreement with our observations of filopodial and cellular dynamics in *ve-cad* and *esama* mutants, as discussed below.

The lack of VE-cad and the additional loss of Esama in tip cell filopodia leads to an increasing disability to generate intercellular contacts. Especially in dKO embryos, the filopodia are going through repetitive cycles of connection. This suggests that in the wild type both proteins are present in the tip cells and mediate EC recognition and adhesion at the onset of anastomosis. The different combinations of mutant alleles can be placed into a phenotypic

Development (2017) 144, 1554-1565 doi:10.1242/dev.140038

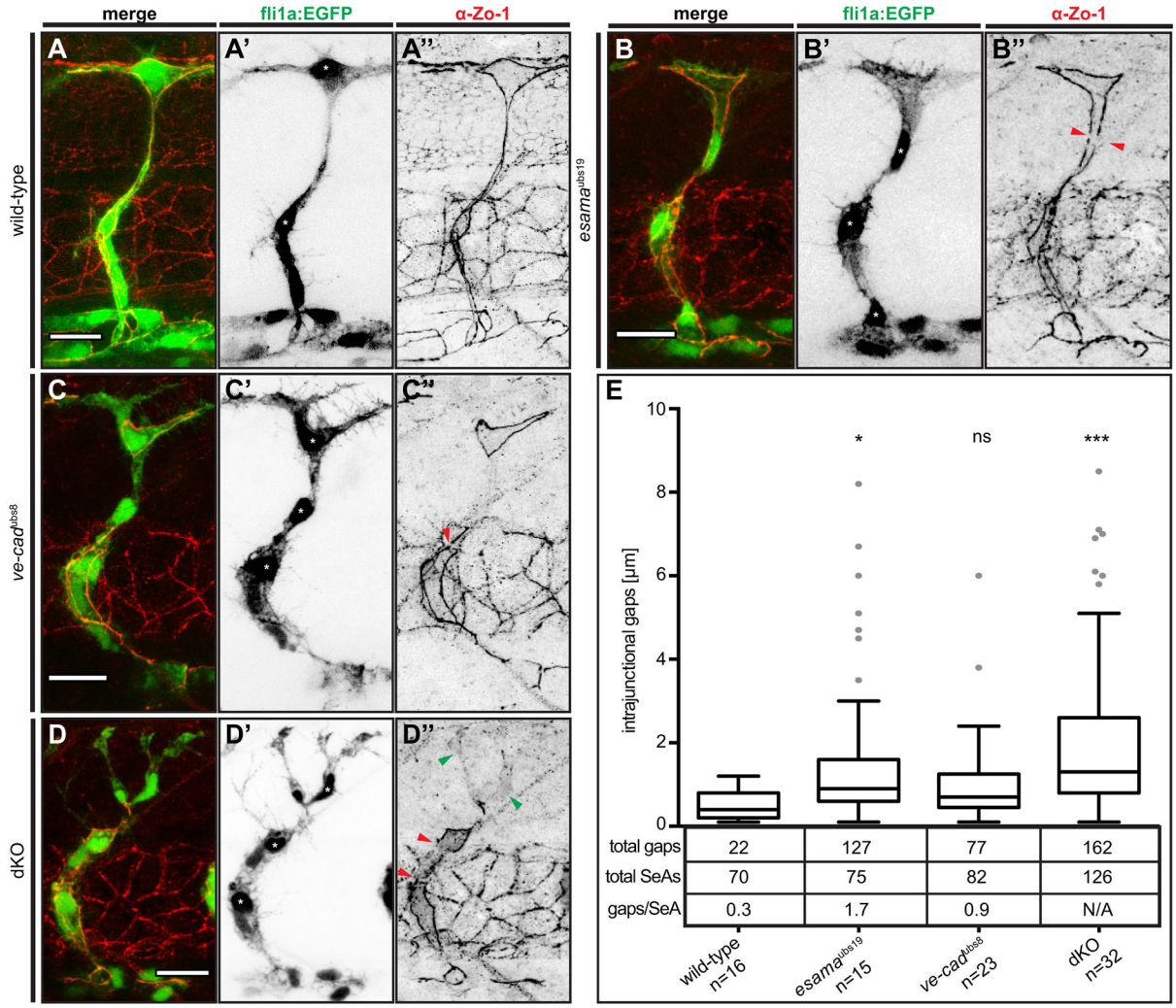

Fig. 5. Defects in junctional continuity in the absence of Esama, which are greatly increased in double mutants. (A-D) Confocal images of SeAs of Tg(*fli1a:EGFP*)^{y1} (green) wild-type (A), *esama*^{ubs19} (B), *ve-cad*^{ubs8} (C) and *esama*^{ubs19}; *ve-cad*^{ubs8} dKO (D) embryos stained for Zo-1 (red), around 32 hpf. Single channels are shown in inversed contrast. Red arrowheads point to intrajunctional gaps or missing junctions between the red arrowheads in (D″); green arrowheads indicate cytoplasmic localization of Zo-1. Asterisk, nucleus. Scale bars: 20 µm. (E) Intrajunctional gaps (in micrometers) measured in confocal projections of embryos stained for Zo-1 around 32 hpf. One-way analysis of variance revealed significance for *esama*^{ubs19} (P=0.0449), *ve-cad*^{ubs8} (P=0.42) and double mutant (P<0.0001). Tukey boxplot shows boxes with lower quartile, median and upper quartile (Tukey whiskers). Medians are 0.4, 0.9, 0.7 and 1.3 µm for wild type, *esama*^{ubs19}, *ve-cad*^{ubs8} and dKO, respectively. The number of observed intrajunctional gaps (total gaps), the number of analyzed SeAs (total SeAs) and the calculated number of intrajunctional gaps per SeA (gaps/SeA) are indicated below the boxplot for every genotype. The number of intrajunctional gaps per SeA is omitted for the double mutant genotype, because strong junctional defects did not allow a quantitative analysis. dKO, double mutant; n, number of embryos analyzed; N/A, not available (omitted); SeA, segmental artery. *P<0.05; ***P<0.001.

series with increasing anastomosis defects. *esama* mutants appear wild-type like, whereas *esama*$^{-/-}$; *ve-cad*$^{+/-}$ and *ve-cad single* mutants exhibit an intermediate phenotype. Lack of both proteins finally disrupts anastomosis almost completely. In this situation, cells accumulate as loose aggregates, indicating that double mutant ECs still retain some cell type-specific adhesiveness. Remarkably, loss of a single copy of *ve-cad* induces mild filopodial defects in homozygous *esama* mutants, suggesting that *esama* mutants are sensitized to *ve-cad* levels. This is in agreement with our qPCR analyses, which show that mRNA levels of *ve-cad* are increased by twofold in *esama* mutants. Taken together, these observations indicate that VE-cad and Esama are partly redundant during anastomosis and that VE-cad can compensate for the loss of Esama, but not vice versa (Fig. S6). Moreover, these observations suggest that the degree of cell type-specific adhesiveness determines the efficacy of anastomosis and thus cell-cell recognition.

Synergistic functions of Esama and VE-cad during angiogenic sprouting

The formation of SeAs is initiated by the activation of ECs in the DA by VEGF-A (Habeck et al., 2002; and reviewed by Siekmann et al., 2013). In general, EC activation is accompanied by a remodeling of the actin cytoskeleton, a reduction in interendothelial adhesion and an increase in motility (Gerhardt et al., 2003; and reviewed by Herbert and Stainier, 2011; van Buul et al., 2014). Nevertheless, junctional proteins, such as Zo-1, Esama and VE-cad, are maintained at cell junctions during SeA sprouting (Blum et al., 2008; Sauteur et al., 2014). In *esama* mutants, SeA formation is almost indistinguishable from wild type. However, the loss of Esama strongly aggravates the defects of *ve-cad* mutants. In *ve-cad* mutants, we have observed two defects within the angiogenic sprout: a detachment of the tip cell from the sprout, which can be attributed to a reduction in interendothelial cell adhesion, and a

Development (2017) 144, 1554-1565 doi:10.1242/dev.140038

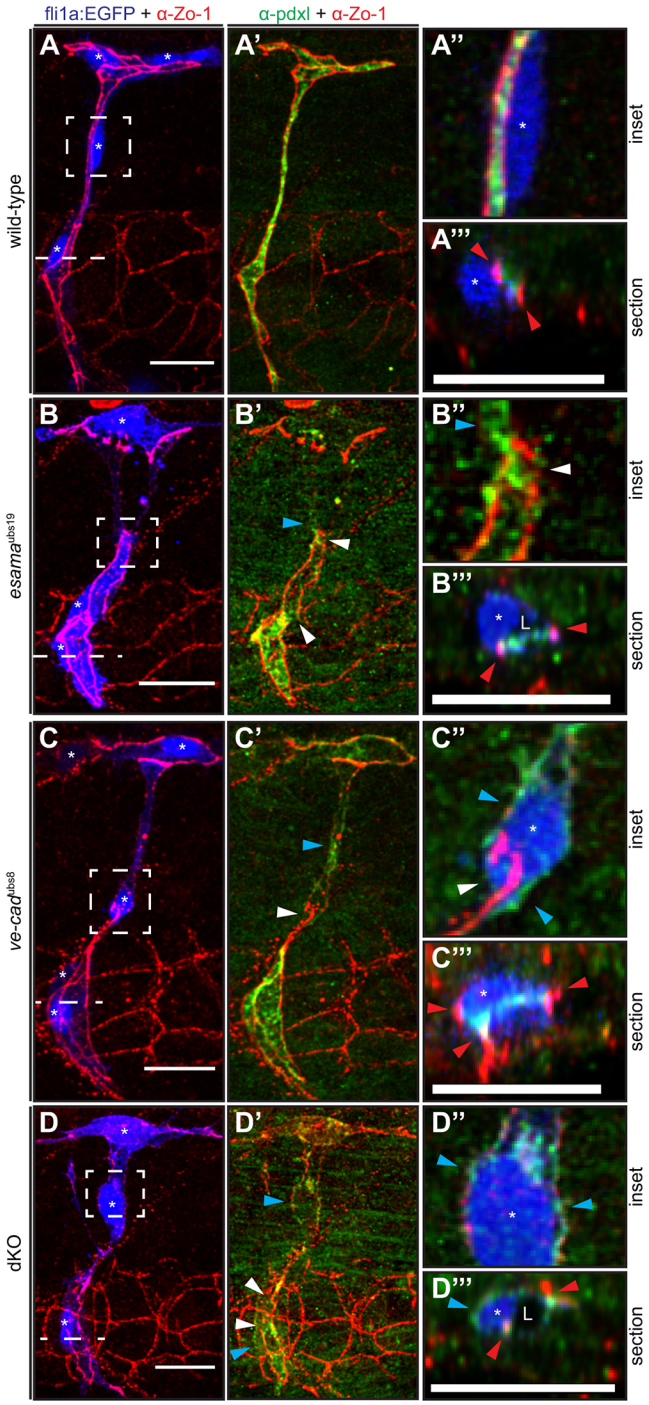

Fig. 6. Intrajunctional gaps are correlated with defects in apical polarization. (A-D) Deconvolved projections of SeAs of Tg(*fli1a:EGFP*)^{y1} (blue) wild-type (A), *esama*^{ubs19} (B), *ve-cad*^{ubs8} (C) and *esama*^{ubs19}; *ve-cad*^{ubs8} double mutant (dKO, D) embryos stained for Zo-1 (red) and Pdxl (green), around 32 hpf. SeAs are shown either in EGFP plus Zo-1 or in Pdxl plus Zo-1 channels, whereas insets and sections are merges of all three colors, except for (B″), where the blue channel was omitted. The panels on the right-hand side represent magnifications and cross-sections of the insets and dotted lines, respectively. Red arrowheads point to junctions; white arrowheads point to intrajunctional gaps or missing junctions between the white arrowheads in (D′); blue arrowheads point to basal localized Pdxl. L, lumen; asterisk, nucleus. Scale bars: 20 µm.

defect in junction/cell elongation within the sprout (Sauteur et al., 2014). The additional loss of Esam appears to enhance primarily the adhesion defects within the sprout. In dKO embryos, ECs in the sprout attain a mesenchymal appearance and their junctional contacts are severely disrupted.

By comparison, the axial vessels, which form by vasculogenesis, are less severely affected by the loss of both proteins. This indicates that dKO ECs still possess cell type-specific adhesive properties, which might be mediated by other endothelium-specific adhesion molecules, such as Claudin 5. However, once dKO ECs have initiated angiogenic sprouting and emigrate from the DA, they start to dissociate. After the ECs have reduced their contacts, they are not able to re-establish an organized endothelium.

In general, our observations support the findings from the mouse Esam knockout, which showed that Esam is not essential for physiological angiogenesis (Ishida et al., 2003). Notably, however, that study also showed an essential role for Esam in tumor angiogenesis and tumor growth. The endothelium of tumor vessels is often disturbed, and ECs are exposed to high levels pro-angiogenic cues (Baluk et al., 2005; Hida et al., 2016). It is therefore conceivable that the tumor environment might affect ECs in a way that mimics the loss of VE-cad and thus makes them susceptible to the additional loss of Esam. In agreement with this notion, knockdown of *ve-cad* in zebrafish can inhibit tumor angiogenesis in xenografts (Nicoli et al., 2007).

Differential roles for Esama and VE-cad in junction formation and apical polarization

In general, our phenotypic analyses indicate that VE-cad function is more vital to cardiovascular development than Esama and that VE-cad can compensate for the loss of Esama during embryonic angiogenesis. We noticed, however, a transient appearance of intrajunctional gaps, which was more pronounced in *esama* than in *ve-cad* mutants (Fig. S6). These gaps were frequent during the early sprouting stages, when junctions are thought to be remodeling extensively, than at later stages, when the lumen was forming. The intrajunctional gaps are associated with a delocalization of Zo-1 from the junction to the cytoplasm and of Pdxl from the apical to the basal cell membrane compartment, which is most obvious in dKOs. The delocalization of Zo-1 is already apparent in *esama*$^{-/-}$; *ve-cad*$^{+/-}$ mutants (data not shown), but is strongly enhanced in dKOs. This finding might be surprising, because Zo-1 has been reported to bind directly to Claudins and JAMs (Fanning and Anderson, 2009) but not to Esam, which binds MAGI-1 (membrane-associated guanylate kinase, WW and PDZ domain-containing protein 1; Magi1 in zebrafish) (Wegmann et al., 2004). However, cell culture experiments suggest that Esam/MAGI-1 interaction activates RhoA, which in turn leads to an accumulation of Zo-1 and F-actin at newly formed junctions (Kimura et al., 2010). Our observations of cytoplasmic Zo-1 accumulation support the view that Esama might have an essential function in recruiting Zo-1 to newly formed or remodeling EC junctions. We cannot exclude alternative explanations, such as that the loss of Esama (plus VE-cad) might lead to more widespread defects in the organization of junctional proteins, which might lead to a loss of direct Zo-1 binding partners at the cell junction.

The redundant functions of VE-cad and Esam during vascular morphogenesis raise the question to what extent these proteins might interact in the same or in separate molecular pathways. Whether Esam and VE-cad physically interact remains to be investigated. Although Esam and VE-cad are localized in different junctional compartments, they might be in close proximity, because tight junctions and adherens junctions of ECs are not strictly segregated (Rüffer et al., 2004; and reviewed by Bazzoni and Dejana, 2004). Both proteins might interact via MAGI-1 and

Development (2017) 144, 1554-1565 doi:10.1242/dev.140038

β-catenin, because Esam has been shown to bind directly to MAGI-1 (Kimura et al., 2010; Wegmann et al., 2004), and VE-cad can bind MAGI-1 through β-catenin (Sakurai et al., 2006).

Taken together, our findings uncover unique and redundant functions of Esama and VE-cad during angiogenic sprouting and anastomosis. VE-cad is essential for contact formation and junctional dynamics during stalk cell elongation and anastomosis. In *esama* mutants, most of the Esama functions can be compensated for by VE-cad. However, the subtle defects in *esama* single mutants point to a unique role of Esama in *de novo* junction formation and maturation.

MATERIALS AND METHODS

Zebrafish lines and maintenance and morpholinos

Zebrafish were maintained in standard conditions (Westerfield, 2000). All experiments were conducted in accordance with federal guidelines and were approved by the Kantonales Veterinäramt of Kanton Basel-Stadt. The zebrafish lines used were as follows: Tg(*fli1a:EGFP*)^{y1} (Lawson and Weinstein, 2002); Tg(*kdrl:mCherry-CAAX*)^{s916} (Hogan et al., 2009); Tg(*fli1ep:gal4ff*)^{ubs3} and Tg(*UAS:EGFP-hsZO-1, cmlc:EGFP*)^{ubs5} (Herwig et al., 2011); Tg(*UAS:EGFP-UCHD*)^{ubs18} and *ve-cad*^{ubs8} (Sauteur et al., 2014); and *esama*^{ubs19} (present study).

Morpholinos (GeneTools) used were as follows: VE-cadherin splice 5′-TTTACAAGACCGTCTACCTTTCCAA-3′ (Nicoli et al., 2007) and standard control 5′-CCTCTTACCTCAGTTACAATTTATA-3′. After imaging, the morphant embryos were stained for VE-cad to verify efficient knockdown. Embryos showing incomplete knockdown were excluded from the analysis.

In situ hybridization

In situ hybridization was performed as described by Thisse and Thisse (2014). To increase the signal, the hybridization mixture was supplemented with 5% dextran sulfate, as described in the protocol.

Images were acquired with a Microphot-FXA (Nikon) microscope, equipped with a Nex-5R (Sony) digital camera, using a 20× dry objective (NA=0.5).

The *esama* antisense template was generated by PCR amplification from the vector cssl:d0254 (Thisse et al., 2008) using T7 polymerase (Roche) for transcription, as described by Thisse et al. (2008).

The *esamb* probe vector was cloned from the cDNA EST clone IMAGp998L2215582Q (GenomeCube, Source BioScience), which was subcloned into the pBluescript II KS backbone. The vector was linearized by *Acc*65I (NEB) for antisense transcription (T7 polymerase; Roche).

Generation and genotyping of the *esama*^{ubs19} mutant line

For the generation of *esama*^{ubs19}, the second exon of the *esama* gene was targeted for mutagenesis. For targeted mutagenesis, TALEN technology was used as described by Cermak et al. (2011). The forward TALEN binds 5′-T-GTTGCCTTATGAAAA-3′ and the reverse TALEN binds 5′-AGAT GGTGGTGCTGC-A-3′ and they are spaced by 20 bp (5′-TGTGGATGT GATCCAAGGGA-3′).

The repeat-variable diresidues (RVDs) of the forward TALEN (NH NG NG NH HD HD NG NG NI NG NH NI NI NI NI) and the reverse TALEN (NH HD NI NH HD NI HD HD NI HD HD NI NG HD NG) were assembled as described by Cermak et al. (2011). Subsequently, the RVD clones were cloned into RCIscript_GoldyTALEN (Bedell et al., 2012), where the T3 promoter was converted to a T7 promoter. The TALEN scaffold vectors were linearized with *Bst*EII (NEB) and *Bsa*I (NEB), gel extracted and transcribed *in vitro* using mMESSAGE mMACHINE T7 ULTRA Transcription Kit (Ambion), according to the manufacturer's protocol. Approximately 600 pg of RNA of each TALEN was coinjected into one-cell stage wild-type eggs. The injected embryos were raised to adulthood. G0 fish were crossed out to wild-type fish, the genomic DNA was extracted by alkaline lysis (Meeker et al., 2007), and the region of interest was amplified by PCR (using primers Pesama_I1_fwd 5′-ATGGTCTTTCAGTCAGCGAG-3′ and Pesama_I2_rev 5′-GTGTGGCAGTTTAATTCAAATC-3′). To screen for mutations, the PCR amplicon was digested with *Sty*I (NEB), which cuts in the spacer region flanked by the TALEN binding sites. Uncut product was sent for sequencing (Microsynth, Switzerland), which revealed a 10 bp deletion. This 10 bp deletion in exon 2 of the *esama* gene leaves the first 37 amino acids of the protein intact and leads to a premature stop codon after another (altered) 33 amino acids (see Fig. S2A).

For genotyping of adult fish or embryos, the genomic DNA from fin biopsies (Meeker et al., 2007) was extracted and genotyped using four primers to discriminate wild-type from heterozygous or homozygous mutant individuals. The combination of four primers (P30 5′-ATGGTCTTT CAGTCAGCGAG-3′, P55 5′-GTGTGGCAGTTTAATTCAAATC-3′, P99 5′-GGATGTGATCCAAGGGAAG-3′ and P101 5′-CCACCATCTTCCCT CCA-3′) generates products of 356 bp for wild-type alleles and 142 bp for mutant alleles (see Fig. S2B,C).

Immunofluorescence

Immunofluorescence was performed as previously described (Herwig et al., 2011). The following antibodies were used: rabbit anti-Esama 1:200 (Sauteur et al., 2014), mouse anti-human-Zo-1 1:100 (Thermo Fisher Scientific, 33-9100), rabbit anti-VE-cad 1:200 (Blum et al., 2008), rabbit anti-Pdxl 1:200 (Herwig et al., 2011), Alexa 568 goat anti-rabbit immunoglobulin (IgG) 1:1000 (A-11011), Alexa 633 goat anti-rabbit IgG 1:1000 (A-21071) and Alexa 633 goat anti-mouse IgG 1:1000 (A-21053) (all secondary antibodies from Invitrogen).

Imaging and image analysis

Fixed or live samples were selected for fluorescence signal, anaesthetized in E3 supplemented with 1× tricaine (0.08%; Sigma) and mounted in a 35 mm glass-bottomed Petri dish (0.17 mm; MatTek), using 0.7% low melting agarose (Sigma) containing 1× tricaine. For live imaging, the mounting agarose was additionally supplemented with 0.003% 1-phenyl-2-thiourea (Sigma). A Leica TCS SP5 confocal microscope was used for time-lapse imaging and images of fixed samples, using 40× (NA=1.1) or 63× (NA=1.2) water immersion objectives. Routinely, *z*-stacks were acquired with a step size of 0.25-0.8 µm, and stacks for time-lapse imaging were acquired every 6-10 min.

High time-resolution movies were acquired with a Perkin Elmer (Ultraview VoX) spinning disk confocal microscope, using a 63× (NA=1.2) water immersion objective. The *z*-stacks were acquired with a step size of 0.3 µm every minute. Subsequently, images were deconvolved using Huygens (SIV). Images and movies were analyzed with ImageJ software (http://fiji.sc/).

Quantification of filopodial protrusions and intrajunctional gaps

Filopodial protrusions were counted in projected confocal stacks of Tg(*fli1ep:gal4ff*)^{ubs3}, Tg(*UAS:EGFP-UCHD*)^{ubs18}, Tg(*kdrl:mCherry-CAAX*)^{s916} embryos of different genotypes, fixed around 32 hpf.

Junctional gaps were measured in projected confocal stacks of embryos of different genotypes, fixed around 32 hpf and stained for Zo-1.

Statistical analysis was performed using Prism software (GraphPad) and ordinary one-way ANOVA with multiple comparisons, corrected with Tukey's test.

RNA extraction from embryos and RT-qPCR analysis

At 32 hpf, wild-type and *esama*^{ubs19} embryos were collected from incrosses, whereas *ve-cad*^{ubs8} and dKO embryos were selected according to their phenotype. Three samples of 15 embryos of each genotype were pooled for RNA extraction. For each genotype, the RNA was extracted using ReliaPrep RNA Cell Miniprep System (Promega) following the manufacturer's instructions.

cDNA was transcribed for 2 h at 37°C from 1 µg RNA using the High Capacity cDNA Reverse Transcription Kit (Applied Biosystems), following the manufacturer's protocol. Subsequently, the cDNA was diluted 1:10.

qPCR was performed using FastStart Universal SYBR green Master (Rox) (Roche) and the ABI 7500 Fast Real-time PCR System (Applied Biosystems). Briefly, 5 µl of the diluted cDNA was mixed with 0.5 µM primers in final 20 µl SYBR green master mix. The cycling program of the qPCR included 10 min initial denaturation at 95°C, followed by 45 cycles of denaturation at 95°C for 10 s and annealing plus extension at 60°C for 30 s.

Development (2017) 144, 1554-1565 doi:10.1242/dev.140038

Experiments were performed for each genotype in three biological and three technical replicates. *rps11* and *beta-actin* were chosen as housekeeping genes, and the fold change of a specific gene was calculated for each genotype. A list of primers is found in Table S1.

Acknowledgements

We thank the Biozentrum Imaging Core Facility for unceasing support. We also thank Drs Ilkka Paatero and Klaus Ebnet for discussions and critical reading of the manuscript.

Competing interests

The authors declare no competing or financial interests.

Author contributions

L.S., M.A. and H.-G.B. conceived the project. L.S. and H.-G.B. designed the experiments. L.S. carried out the experiments. L.S., M.A. and H.-G.B. analyzed the data. L.S. and H.-G.B. wrote the manuscript.

Funding

L.S. was supported by a fellowship from the Werner Siemens-Stiftung. This work was supported by the Basel-Stadt and Basel-Land Kantons and by a grant from the Schweizerischer Nationalfonds zur Förderung der Wissenschaftlichen Forschung (156838 to M.A.).

Supplementary information

Supplementary information available online at
http://dev.biologists.org/lookup/doi/10.1242/dev.140038.supplemental

References

Baluk, P., Hashizume, H. and McDonald, D. M. (2005). Cellular abnormalities of blood vessels as targets in cancer. *Curr. Opin. Genet. Dev.* **15**, 102-111.

Bazzoni, G. and Dejana, E. (2004). Endothelial cell-to-cell junctions: molecular organization and role in vascular homeostasis. *Physiol. Rev.* **84**, 869-901.

Bedell, V. M., Wang, Y., Campbell, J. M., Poshusta, T. L., Starker, C. G., Krug, R. G., II, Tan, W., Penheiter, S. G., Ma, A. C., Leung, A. Y. H. et al. (2012). *In vivo* genome editing using a high-efficiency TALEN system. *Nature* **491**, 114-118.

Betz, C., Lenard, A., Belting, H.-G. and Affolter, M. (2016). Cell behaviors and dynamics during angiogenesis. *Development* **143**, 2249-2260.

Blum, Y., Belting, H.-G., Ellertsdottir, E., Herwig, L., Lüders, F. and Affolter, M. (2008). Complex cell rearrangements during intersegmental vessel sprouting and vessel fusion in the zebrafish embryo. *Dev. Biol.* **316**, 312-322.

Carmeliet, P., Lampugnani, M.-G., Moons, L., Breviario, F., Compernolle, V., Bono, F., Balconi, G., Spagnuolo, R., Oosthuyse, B., Dewerchin, M. et al. (1999). Targeted deficiency or cytosolic truncation of the VE-cadherin gene in mice impairs VEGF-mediated endothelial survival and angiogenesis. *Cell* **98**, 147-157.

Cermak, T., Doyle, E. L., Christian, M., Wang, L., Zhang, Y., Schmidt, C., Baller, J. A., Somia, N. V., Bogdanove, A. J. and Voytas, D. F. (2011). Efficient design and assembly of custom TALEN and other TAL effector-based constructs for DNA targeting. *Nucleic Acids Res.* **39**, e82.

Chaki, S. P., Barhoumi, R. and Rivera, G. M. (2015). Actin remodeling by Nck regulates endothelial lumen formation. *Mol. Biol. Cell* **26**, 3047-3060.

Dejana, E. (2004). Endothelial cell–cell junctions: happy together. *Nat. Rev. Mol. Cell Biol.* **5**, 261-270.

Dejana, E. and Vestweber, D. (2013). The role of VE-cadherin in vascular morphogenesis and permeability control. *Prog. Mol. Biol. Transl. Sci.* **116**, 119-144.

Fanning, A. S. and Anderson, J. M. (2009). Zonula occludens-1 and -2 are cytosolic scaffolds that regulate the assembly of cellular junctions. *Ann. N. Y. Acad. Sci.* **1165**, 113-120.

Gerhardt, H., Golding, M., Fruttiger, M., Ruhrberg, C., Lundkvist, A., Abramsson, A., Jeltsch, M., Mitchell, C., Alitalo, K., Shima, D. et al. (2003). VEGF guides angiogenic sprouting utilizing endothelial tip cell filopodia. *J. Cell Biol.* **161**, 1163-1177.

Gory-Fauré, S., Prandini, M. H., Pointu, H., Roullot, V., Pignot-Paintrand, I., Vernet, M. and Huber, P. (1999). Role of vascular endothelial-cadherin in vascular morphogenesis. *Development* **126**, 2093-2102.

Habeck, H., Odenthal, J., Walderich, B., Maischein, H.-M. and Schulte-Merker, S. and **Tübingen 2000 screen consortium**. (2002). Analysis of a zebrafish VEGF receptor mutant reveals specific disruption of angiogenesis. *Curr. Biol.* **12**, 1405-1412.

Herbert, S. P. and Stainier, D. Y. R. (2011). Molecular control of endothelial cell behaviour during blood vessel morphogenesis. *Nat. Rev. Mol. Cell Biol.* **12**, 551-564.

Herwig, L., Blum, Y., Krudewig, A., Ellertsdottir, E., Lenard, A., Belting, H.-G. and Affolter, M. (2011). Distinct cellular mechanisms of blood vessel fusion in the zebrafish embryo. *Curr. Biol.* **21**, 1942-1948.

Hida, K., Maishi, N., Torii, C. and Hida, Y. (2016). Tumor angiogenesis—characteristics of tumor endothelial cells. *Int. J. Clin. Oncol.* **21**, 206-212.

Hirata, K.-i., Ishida, T., Penta, K., Rezaee, M., Yang, E., Wohlgemuth, J. and Quertermous, T. (2001). Cloning of an immunoglobulin family adhesion molecule selectively expressed by endothelial cells. *J. Biol. Chem.* **276**, 16223-16231.

Hogan, B. M., Bos, F. L., Bussmann, J., Witte, M., Chi, N. C., Duckers, H. J. and Schulte-Merker, S. (2009). *ccbe1* is required for embryonic lymphangiogenesis and venous sprouting. *Nat. Genet.* **41**, 396-398.

Ishida, T., Kundu, R. K., Yang, E., Hirata, K.-i., Ho, Y.-D. and Quertermous, T. (2003). Targeted disruption of endothelial cell-selective adhesion molecule inhibits angiogenic processes *in vitro* and *in vivo*. *J. Biol. Chem.* **278**, 34598-34604.

Khandoga, A., Huettinger, S., Khandoga, A. G., Li, H., Butz, S., Jauch, K.-W., Vestweber, D. and Krombach, F. (2009). Leukocyte transmigration in inflamed liver: a role for endothelial cell-selective adhesion molecule. *J Hepatol.* **50**, 755-765.

Kimura, R., Ishida, T., Kuriyama, M., Hirata, K.-i. and Hayashi, Y. (2010). Interaction of endothelial cell-selective adhesion molecule and MAGI-1 promotes mature cell-cell adhesion via activation of RhoA. *Genes Cells* **15**, 385-396.

Lagendijk, A. K. and Hogan, B. M. (2015). VE-cadherin in vascular development: a coordinator of cell signaling and tissue morphogenesis. *Curr. Top. Dev. Biol.* **112**, 325-352.

Lampugnani, M. G., Orsenigo, F., Rudini, N., Maddaluno, L., Boulday, G., Chapon, F. and Dejana, E. (2010). CCM1 regulates vascular-lumen organization by inducing endothelial polarity. *J. Cell Sci.* **123**, 1073-1080.

Lawson, N. D. and Weinstein, B. M. (2002). *In vivo* imaging of embryonic vascular development using transgenic zebrafish. *Dev. Biol.* **248**, 307-318.

Lenard, A., Ellertsdottir, E., Herwig, L., Krudewig, A., Sauteur, L., Belting, H.-G. and Affolter, M. (2013). In vivo analysis reveals a highly stereotypic morphogenetic pathway of vascular anastomosis. *Dev. Cell* **25**, 492-506.

Leslie, J. D., Ariza-McNaughton, L., Bermange, A. L., McAdow, R., Johnson, S. L. and Lewis, J. (2007). Endothelial signalling by the Notch ligand Delta-like 4 restricts angiogenesis. *Development* **134**, 839-844.

Luissint, A.-C., Nusrat, A. and Parkos, C. A. (2014). JAM-related proteins in mucosal homeostasis and inflammation. *Semin. Immunopathol.* **36**, 211-226.

Meeker, N. D., Hutchinson, S. A., Ho, L. and Trede, N. S. (2007). Method for isolation of PCR-ready genomic DNA from zebrafish tissues. *BioTechniques* **43**, 610, 612, 614.

Montero-Balaguer, M., Swirsding, K., Orsenigo, F., Cotelli, F., Mione, M. and Dejana, E. (2009). Stable vascular connections and remodeling require full expression of VE-cadherin in zebrafish embryos. *PLoS ONE* **4**, e5772.

Nasdala, I., Wolburg-Buchholz, K., Wolburg, H., Kuhn, A., Ebnet, K., Brachtendorf, G., Samulowitz, U., Kuster, B., Engelhardt, B., Vestweber, D. et al. (2002). A transmembrane tight junction protein selectively expressed on endothelial cells and platelets. *J. Biol. Chem.* **277**, 16294-16303.

Nicoli, S., Ribatti, D., Cotelli, F. and Presta, M. (2007). Mammalian tumor xenografts induce neovascularization in zebrafish embryos. *Cancer Res.* **67**, 2927-2931.

Phng, L.-K., Stanchi, F. and Gerhardt, H. (2013). Filopodia are dispensable for endothelial tip cell guidance. *Development* **140**, 4031-4040.

Phng, L.-K., Gebala, V., Bentley, K., Philippides, A., Wacker, A., Mathivet, T., Sauteur, L., Stanchi, F., Belting, H.-G., Affolter, M. et al. (2015). Formin-mediated actin polymerization at endothelial junctions is required for vessel lumen formation and stabilization. *Dev. Cell* **32**, 123-132.

Rüffer, C., Strey, A., Janning, A., Kim, K. S. and Gerke, V. (2004). Cell–cell junctions of dermal microvascular endothelial cells contain tight and adherens junction proteins in spatial proximity. *Biochemistry* **43**, 5360-5369.

Sakurai, A., Fukuhara, S., Yamagishi, A., Sako, K., Kamioka, Y., Masuda, M., Nakaoka, Y. and Mochizuki, N. (2006). MAGI-1 is required for Rap1 activation upon cell-cell contact and for enhancement of vascular endothelial cadherin-mediated cell adhesion. *Mol. Biol. Cell* **17**, 966-976.

Sauteur, L., Krudewig, A., Herwig, L., Ehrenfeuchter, N., Lenard, A., Affolter, M. and Belting, H.-G. (2014). Cdh5/VE-cadherin promotes endothelial cell interface elongation via cortical actin polymerization during angiogenic sprouting. *Cell Rep.* **9**, 504-513.

Schuermann, A., Helker, C. S. M. and Herzog, W. (2014). Angiogenesis in zebrafish. *Semin. Cell Dev. Biol.* **31**, 106-114.

Siekmann, A. F. and Lawson, N. D. (2007). Notch signalling limits angiogenic cell behaviour in developing zebrafish arteries. *Nature* **445**, 781-784.

Siekmann, A. F., Affolter, M. and Belting, H.-G. (2013). The tip cell concept 10 years after: new players tune in for a common theme. *Exp. Cell Res.* **319**, 1255-1263.

Strilić, B., Kucera, T., Eglinger, J., Hughes, M. R., McNagny, K. M., Tsukita, S., Dejana, E., Ferrara, N. and Lammert, E. (2009). The molecular basis of vascular lumen formation in the developing mouse aorta. *Dev. Cell* **17**, 505-515.

Development (2017) 144, 1554-1565 doi:10.1242/dev.140038

Strilić, B., Eglinger, J., Krieg, M., Zeeb, M., Axnick, J., Babál, P., Müller, D. J. and Lammert, E. (2010). Electrostatic cell-surface repulsion initiates lumen formation in developing blood vessels. *Curr. Biol.* **20**, 2003-2009.

Thisse, B. and Thisse, C. (2014). In situ hybridization on whole-mount zebrafish embryos and young larvae. *Methods Mol. Biol.* **1211**, 53-67.

Thisse, B., Wright, J. G., Wright, J. G. and Thisse, C. (2008). *Embryonic and Larval Expression Patterns from a Large Scale Screening for Novel Low Affinity Extracellular Protein Interactions*. ZFIN Direct Data Submission (http://zfin.org).

van Buul, J. D., Geerts, D. and Huveneers, S. (2014). Rho GAPs and GEFs: controling switches in endothelial cell adhesion. *Cell Adh Migr* **8**, 108-124.

Wacker, A. and Gerhardt, H. (2011). Endothelial development taking shape. *Curr. Opin. Cell Biol.* **23**, 676-685.

Wegmann, F., Ebnet, K., Du Pasquier, L., Vestweber, D. and Butz, S. (2004). Endothelial adhesion molecule ESAM binds directly to the multidomain adaptor MAGI-1 and recruits it to cell contacts. *Exp. Cell Res.* **300**, 121-133.

Wegmann, F., Petri, B., Khandoga, A. G., Moser, C., Khandoga, A., Volkery, S., Li, H., Nasdala, I., Brandau, O., Fässler, R. et al. (2006). ESAM supports neutrophil extravasation, activation of Rho, and VEGF-induced vascular permeability. *J. Exp. Med.* **203**, 1671-1677.

Westerfield, M. (2000). *The Zebrafish Book: a Guide for the Laboratory Use of Zebrafish Danio rerio*. Eugene, OR: University of Oregon Press.

Wong, K. S., Proulx, K., Rost, M. S. and Sumanas, S. (2009). Identification of vasculature-specific genes by microarray analysis of Etsrp/Etv2 overexpressing zebrafish embryos. *Dev. Dyn.* **238**, 1836-1850.